Key Points:
- Video footage shows tsunami inundation within 1-2 min after the mainshock with periods shorter than those recorded by the local tide gauge
- Published rupture models predict up to 5-m tsunami runups but cannot explain their timing, amplitude, and period as reconstructed from videos
- Videos reveal key role of suitably designed escape routes and vertical platforms for timely self-evacuation from rapid tsunami inundation

Nearly Instantaneous Tsunamis Following the *Mw* 7.5 2018 Palu Earthquake

Matías Carvajal[1,2] (iD), **Cristian Araya-Cornejo[3]**, **Ignacio Sepúlveda[4]** (iD), **Daniel Melnick[2,5]** (iD), and **Jennifer S. Haase[4]** (iD)

[1]Programa de Doctorado en Ciencias Geológicas, Facultad de Ciencias Químicas, Universidad de Concepción, Concepción, Chile, [2]Millennium Nucleus The Seismic Cycle Along Subduction Zones, Valdivia, Chile, [3]Observatorio en Gestión del Riesgo de Desastres, Universidad Bernardo O'Higgins, Santiago, Chile, [4]Cecil H. and Ida M. Green Institute of Geophysics and Planetary Physics, Scripps Institution of Oceanography, University of California, San Diego, La Jolla, CA, USA, [5]Instituto de Ciencias de la Tierra, Universidad Austral de Chile, Valdivia, Chile

Abstract The tsunami observations produced by the 2018 magnitude 7.5 Palu strike-slip earthquake challenged the traditional basis underlying tsunami hazard assessments and early warning systems. We analyzed an extraordinary collection of 38 amateur and closed circuit television videos to show that the Palu tsunamis devastated widely separated coastal areas around Palu Bay within a few minutes after the mainshock and included wave periods shorter than 100 s missed by the local tide station. Although rupture models based on teleseismic and geodetic data predict up to 5-m tsunami runups, they cannot explain the higher surveyed runups nor the tsunami waveforms reconstructed from video footage, suggesting either these underestimate actual seafloor deformation and/or that non-tectonic sources were involved. Post-tsunami coastline surveys combined with video evidence and modeled tsunami travel times suggest that submarine landslides contributed to tsunami generation. The video-based observations have broad implications for tsunami hazard assessments, early warning systems, and risk-reduction planning.

Plain Language Summary Tsunami hazard assessment is routinely based on assessing the impacts of long-period waves generated by vertical seafloor motions reaching the coast tens of minutes after the earthquake in typical subduction-zone environments. This view is inadequate for assessing hazard associated with strike-slip earthquakes such as the magnitude 7.5 2018 Palu earthquake, which resulted in tsunami effects much larger than would normally be associated with horizontal fault motion. From an extraordinary collection of 38 amateur and closed circuit television videos we estimated tsunami arrival times, amplitudes, and wave periods at different locations around Palu Bay, where the most damaging waves were reported. We found that the Palu tsunamis devastated widely separated coastal areas within a few minutes after the mainshock and included unusually short wave periods, which cannot be explained by the earthquake fault slip alone. Post-tsunami surveys show changes in the coastline, and this combined with video footage provides potential locations of submarine landslides as tsunami sources that would match the arrival times of the waves. Our results emphasize the importance of estimating tsunami hazards along coastlines bordering strike-slip fault systems and have broad implications for considering shorter-period nearly instantaneous tsunamis in hazard mitigation and tsunami early warning systems.

1. Introduction

Sulawesi Island in the central part of Indonesia is located in a complex tectonic setting where the Australian, Sunda, and Philippine plates meet in a triple junction (Socquet et al., 2006; Walpersdorf et al., 1998). This region is characterized by distributed deformation over a broad region, which can be explained by block rotations along active faults with variable kinematics. Earthquake and tsunami events have repeatedly affected this region in the recorded history (Katili, 1970). The most recent tsunami occurred on the evening of 28 September 2018, at 18:02:45, local time (UTC+8), when a moment magnitude (*Mw*) 7.5 earthquake ruptured a ~200-km-long segment of the Palu-Koro strike-slip fault, which bisects Sulawesi and connects with the Minahassa Trench in the north (Bellier et al., 2001; Socquet et al., 2006; Walpersdorf et al., 1998; Watkinson et al., 2012; Watkinson & Hall, 2017; Figure 1a). In this region, three tsunamigenic earthquakes were reported in the past century (1927, 1968, and 1996) with accompanying tsunamis of up to 10 m (Soloviev & Go, 1974), most of them presumably associated with vertical motions caused by either thrust or normal faulting (Prasetya et al., 2001). In contrast, the Palu earthquake was associated with horizontal
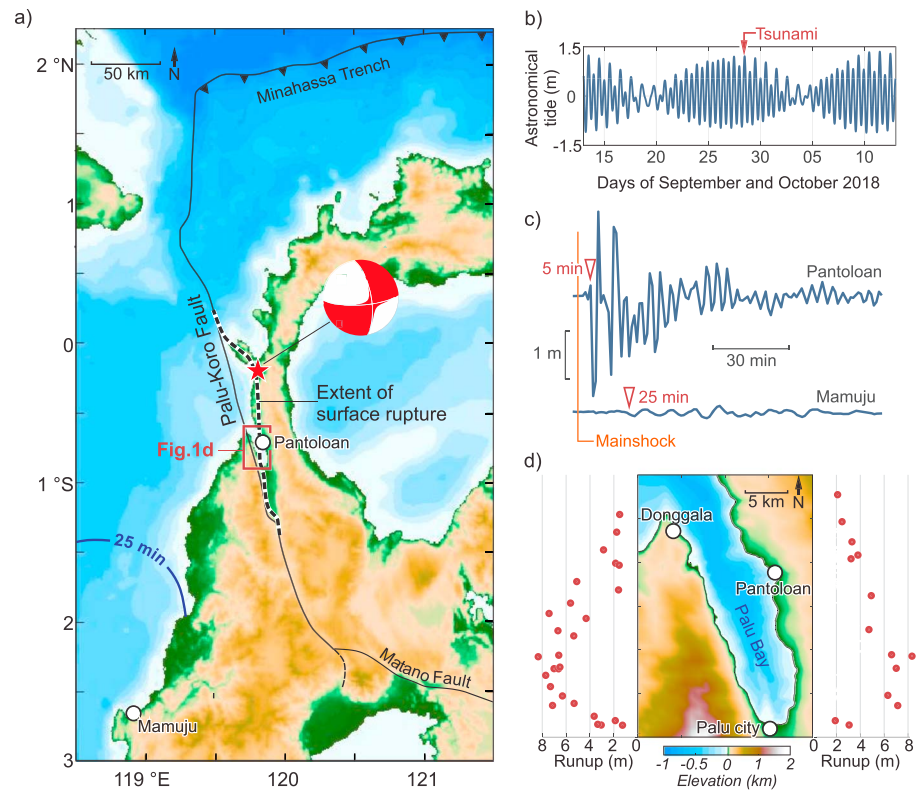
Figure 1. Seismotectonic setting and tsunami observations. (a) Tectonic setting and proposed earthquake rupture of the *Mw* 7.5 strike-slip Palu earthquake (Socquet et al., 2019). Black dashed line indicates the surface rupture proposed by Socquet et al. (2019); red star denotes the epicenter and focal mechanism from USGS (2018). Blue isoline indicates 25-min travel time for a point source tsunami originating at Mamuju. (b) Timing of the tsunami relative to 30 days of predicted astronomical tides for Palu Bay. Note that the tsunami occurred during a high tide of ~1 m above mean sea level. (c) De-tided records of the Palu tsunamis at Pantoloan and Mamuju. The arrival times of the first evident perturbations are indicated in reddish triangles. (d) Topobathymetric map of Palu Bay (Informasi Geospasial, 2018a) and surveyed tsunami runup heights (Fritz et al., 2018).

motion caused by strike-slip faulting. Rupture models based on distant teleseismic waveforms (U.S. Geological Survey, USGS, 2018) and onshore space geodesy data (Socquet et al., 2019) consistently indicate up to ~7 m of horizontal slip confined above 10-km depth with local dip-slip motion of up to only 2 m (Socquet et al., 2019).

Large tsunamis following the Palu earthquake rapidly attracted the attention of the scientific community. Although strike-slip earthquakes have caused historical (Imamura et al., 1995) and recent tsunamis (Hornbach et al., 2010), their amplitudes were much smaller than those observed around Palu Bay, where runups over 8 m were measured in field surveys (Figure 1d; Fritz et al., 2018; Muhari et al., 2018; Omira et al., 2019). This suggests that (i) despite its predominant strike-slip mechanism, the earthquake was capable of producing significant, coseismic vertical deformation beneath the bay, (ii) that tsunami waves were largely amplified by the unusual bathymetric features of the long and narrow bay (Figure 1d), and/or (iii) that additional non-tectonic sources contributed to tsunami generation. To gain insight into this problem, Heidarzadeh et al. (2019) compared tsunami waveforms predicted by numerical modeling with the two closest tide gauge records available for this event (Pantoloan and Mamuju, Figure 1c). They suggested that additional tsunami sources were required and that submarine landslides were the most reasonable candidates. However, these results were likely biased by the use of GEBCO bathymetry for tsunami modeling, which in some locations shows water depths 3 times smaller than those reported on higher-resolution charts (Informasi Geospasial, 2018a). Moreover, their analysis relied only on the Pantoloan tide gauge record (Figure 1c), which is relatively far (15 km) from the area affected by the largest waves (Figure 1d).

Here, we complement the Pantoloan tide gauge data with non-conventional evidence inferred from a novel approach that combines the analysis of video footage and satellite imagery. We used an extraordinary

collection of video images that captured different phases of the tsunami event (i.e., formation, propagation, and inundation) to derive quantitative estimates of their amplitudes, periods and timing around Palu Bay. Our analysis provides temporal data that is not possible to recover in field surveys (Fritz et al., 2018; Muhari et al., 2018; Omira et al., 2019). By tracking sea level changes from image pixels in subsequent frames, we constructed accurately timed tsunami waveforms from the quantitative interpretation of video footage (e.g., Fritz et al., 2006, 2012; Koshimura & Hayashi, 2012). In addition to providing valuable observations to constrain further source studies, we show that hazardous, short-period tsunamis struck nearly instantaneously with the seismic shaking at several locations around the bay and that these short-period waves were not recorded by the Pantoloan tide gauge station due to its longer sampling interval.

2. Video-Based Characterization of the Palu Tsunamis

Our extensive search on social media platforms resulted in 38 videos showing tsunami behavior at 14 sites around Palu Bay (white and magenta circles on Figure 2a; Table S1 and Data Set S1 in the supporting information), from which 23 provide relevant spatiotemporal information at six sites that can be used to reconstruct tsunami waveforms (Table S2 and Text S1). All videos were further used to support the satellite imagery analysis conducted to derive inundation distances around Palu Bay. We will refer to these videos by the names shown in Figure 2a and Table S1. The richness of tsunami information depends on the quantity and quality of the videos, which differ substantially among locations. While tsunamis at some places were observed by a single amateur video, others were precisely captured by several closed circuit television (CCTV) cameras.

In Figure 2b, the waveforms derived from video footage show the tsunami amplitude and timing at six locations (see Data Set S2 for waveform data). For reference we show the simulated tsunami waveforms predicted from the Socquet et al. (2019; blue) and USGS (2018; tan) earthquake rupture models. The tsunami occurred at high tide, corresponding to ~1 m above mean sea level (MSL). The vertical coseismic seafloor deformation generated by the source model at each location added to the tidal value gives the initial sea surface elevation above MSL shown in the figure. For example, at Dupa, the Socquet et al. (2019) model, which concentrates slip beneath the center of the bay, predicts negligible vertical coseismic deformation and therefore the initial value is nearly the tidal level (i.e., 1 m above MSL). On the other hand, the USGS (2018) model predicts significant coseismic subsidence of the seafloor at Dupa; therefore, the water drops with the land instantaneously in our simulations, producing an initial sea level of approximately 0.5 m above MSL. See Text S1 for the details of the waveform reconstruction procedure.

Probably the most remarkable features of the tsunamis that devastated Palu were the very short, nearly instantaneous arrival times. Usually, it is assumed that the time lag between an earthquake and its associated tsunami spans from tens of minutes to several hours (Cienfuegos et al., 2018; Mori et al., 2011), depending on the distance to the source region. However, CCTV footage from the Kampung Nelayan Hotel (KN Hotel), on the southeast coast of Palu Bay, recorded devastating tsunamis arriving 100 s after the seismic shaking (videos 1–6 and compiled video 42, Text S2, and Figure S1). This extremely short arrival time is robustly estimated by the difference in the timing between seismic shaking and water inundation using three cameras that had a clear view of the coastline (videos 1–3). Another array of CCTV cameras at Wani, located 20 km north of KN Hotel, showed tsunami inundation 3.5 min after the seismic shaking, which include the time needed for the tsunami to reach the site located 150 m inland (videos 7 and 8, Text S3, and Figure S2). If we assume a typical 5-m/s inundation rate, a positive-polarity wave (water level rise) should have reached the coast of Wani about 3 min after the mainshock (Figure 2b). Such an inference is consistent with reports from crewmembers of a passenger ship that was stranded on the adjacent coast (Figure S2 and video 9), who unanimously reported that immediately after the earthquake the sea level retreated significantly and was followed 3–5 min later by a large wave (Associated Press, 2018; Chicago Tribune, 2018; Text S3). This sea level pattern is consistent with the vertical movements of a container ship berthed at the Pantoloan port, 2.5 km south of Wani. There, a CCTV camera recorded more than ~2 m of water drawdown ~3 min after the end of seismic shaking followed by a rapid sea level rise of at least ~4 m (Figure 2b, video 11, Text S4, and Figure S3). In summary, videos collected at the KN Hotel, Wani, and Pantoloan (~20-km maximum separation) indicate rapid widespread tsunami inundation following the earthquake and provide valuable reconstructions of tsunami sea level waveforms at these locations (Figure 2b).
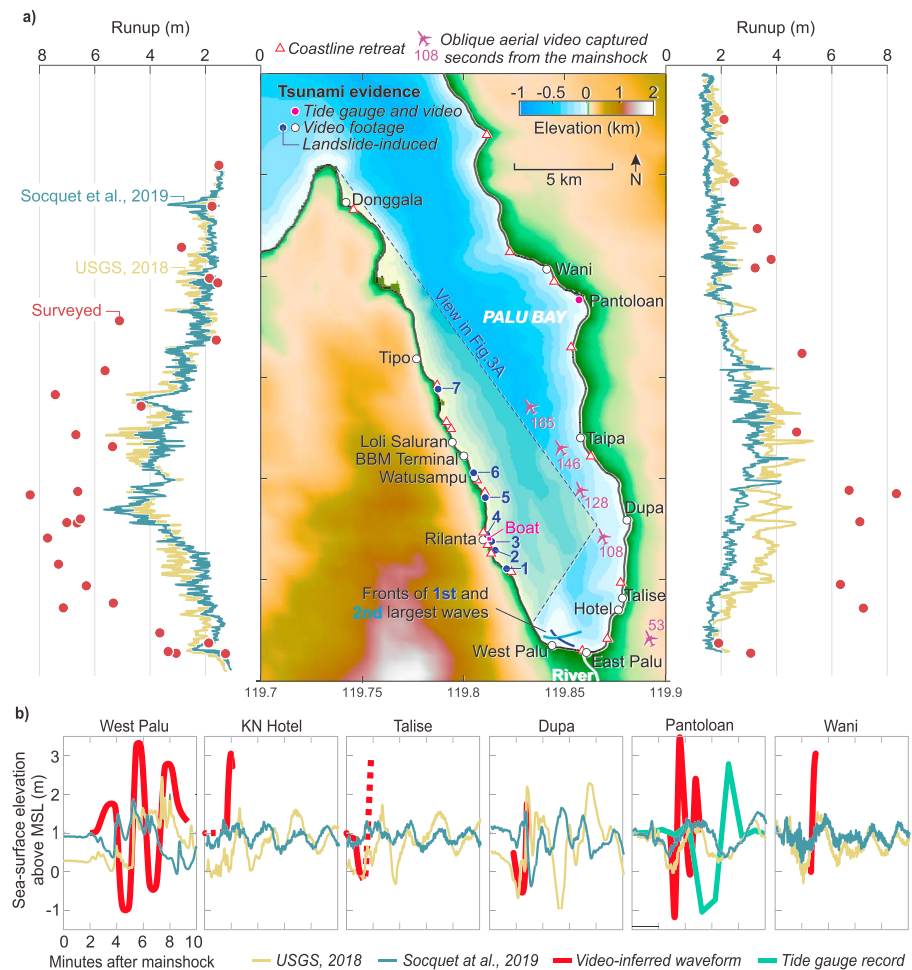
Figure 2. Observations and modeling results. (a) Map showing tsunami video location names (white and magenta circles), location of coastline retreat identified from satellite imagery (triangles), and flight path and timing (in seconds after the mainshock) of the aircraft pilot who recorded the point-source tsunamis shown in Figure 3a (video 38). The left and right panels show a comparison of tsunami runups measured by field surveys (Fritz et al., 2018) with those simulated based on existing coseismic slip models (Socquet et al., 2019; USGS, 2018). (b) Tsunami waveforms reconstructed from video footage (red) and predicted by the Socquet et al. (2019; blue) and USGS (2018; tan) coseismic slip models. The red dashed lines represent the waveform segments interpreted from videos with lower confidence (see text). Tsunami waveforms (available in Data Set S2) were inferred using videos 15–21 at Palu west (see video compilation 43), videos 1–3 at the KN Hotel (see video compilation 42), video 13 at Talise, video 14 at Dupa, video 11 at Pantoloan, and videos 7 and 8 at Wani (Table S2). Note the longer period waveform of the Pantoloan tide gauge record (green) with respect to the waveform reconstructed from closed circuit television footage (red). Tsunami simulations (runups in a and waveforms in b) and the video-inferred tsunami waveforms (b) are plotted as sea surface elevation including the high tide level of ~1 m above mean sea level at the time of the earthquake (Figure 1b).

Negative-polarity waves (water level drawdown) occurring immediately after the earthquake followed by tsunami inundation were observed at some sites but were not ubiquitous around the bay. For example, at Talise, an evident water retreat occurred almost instantaneously with seismic shaking (continuous red line in the Talise waveform of Figure 2b), which then appeared to be followed by a large wave that spurred people to run landward (dashed red line in the Talise waveform of Figure 2b; video 13). A very similar spatiotemporal behavior of sea level appeared to occur ~4 km north at Dupa, where a tsunami bore rapidly formed after an evident water drawdown (Figure 2b and video 14). However, negative-polarity leading waves followed by bore fronts, if existed, were not evident in the CCTV videos at the KN Hotel (see video 3), which is located 5 km south of Dupa and only 1 km from Talise. Instead, we infer an initial positive inundation from a rapid sea level increase of at least 2 m (Figure 2b and video 3).

Bore-type tsunamis followed by water retreat characterized the tsunamis that devastated the western parts of Palu city. Here, the tsunamis were captured by seven amateur videos collected within the Palu Grand Mall (videos 15–21 and compiled video 43 and Figure S4). The videos complement each other, in terms of view angles and temporal windows, and we were thus able to construct a quantitative composite estimate of arrival time, amplitudes and wave periods (Figure 2b). The video analysis shows that most of the destruction throughout Palu city was caused by two large tsunami waves arriving after smaller, but still significant, leading waves (Figures 2b and S4). Both of the largest waves featured evident bore fronts and impacted the coast from significantly different directions; first from the northeast and then from the northwest (Figures 2a and S4). Although no CCTV cameras recorded the exact tsunami arrival time at Palu city, the panic on the scene observed at the beginning of videos 15 and 16 strongly suggests that the leading, smaller waves likely arrived less than 2 min after the earthquake. Because the first and second large trailing waves impacted 2 and 4 min after these initial inundations, respectively, the western sector of Palu city was likely devastated within 4–6 min of the mainshock, which is consistent with precise video observations at KN Hotel, Wani, and Pantoloan. Interestingly, if a single tsunami source is considered, the time span between waves at Palu city is consistent with a wave train period of ~2 min, which is unusually short for typical tectonic tsunamis (eg., Ward, 2011). Alternatively, the tsunamis that hit Palu city may have been caused by different sources, as suggested by their contrasting incoming directions.

Tsunami wavefronts impacting the local coastline with different orientations were apparently a hallmark of the Palu event, possibly produced by refraction in the shoaling of the waves due to the coastal bathymetry and/or by non-tectonic sources occurring close to the coast where observations were made. For instance, westward, coast-parallel inundation was captured by amateur videos in the eastern sectors of Palu city (videos 22 and 23). The KN Hotel CCTV footage simultaneously captured both eastward (videos 3 and 6) and westward (videos 1 and 2) inundations (Figure S1 and video 42). Unfortunately, the inundation at KN Hotel was nearly perpendicular to the evacuation road (video 6). This, combined with the nearly instantaneous arrivals (~100 s), prevented a successful evacuation (Figure S1). On the other hand, the fortunate orientation of the road perpendicular to the coastline near the Wani house allowed timely self-evacuations even from rapid tsunami arrivals (see Text S3). Vertical evacuation proved to be critical in areas where there was insufficient time available to evacuate horizontally, as revealed by video footage at the KN Hotel (video 4), eastern (videos 23 and 25–27), and western Palu (videos 1 and 5). The video analysis highlights the importance of addressing the possible directions of tsunami inundation in hazard assessments and their mitigation in planning evacuation routes, including vertical platforms if necessary, to reduce loss of life.

Overall, our video-based observations are consistent with high-amplitude tsunamis with sources near the coast (short arrival times), with unusually short periods (~2 min) and consequently short wavelengths. These tsunami characteristics resulted in rather high destructive capacity but limited capacity to inundate far inland (Satake et al., 2013). These characteristics are consistent with inland inundation distances inferred from satellite imagery (Figure S5), which provide a regional-scale assessment. Our interpretation of high-resolution satellite images collected 3 to 4 days after the event (Digital Globe, 2018) suggests that severe devastation was confined to at most ~400 m inland (Figure S5). These characteristics are also consistent with the time-frequency signature of the Pantoloan tide gauge record, which shows that most of the initial energy was limited to 2- to 6-min periods (Figure S6). However, we note that the 1-min sampling interval of the Pantoloan record, which would usually be sufficient for characterizing subduction zone tsunamis, may be too coarse for capturing the tsunami patterns inferred from CCTV footage collected in the vicinity of the tide gauge station (video 11 and Figure S3). The vertical movements of the berthed container ship at Pantoloan port observed in video 11 are best explained by two tsunami waves (two troughs and two crests) occurring within less than 5 min after seismic shaking stopped (Figure S3). Interestingly, these waves were not captured by the local tide gauge station, which recorded longer-period fluctuations (~6 min) beginning with a leading drawdown at ~5 min following the mainshock (Figures 1c, 2b, and S6). Hence, our observations suggest that the Palu tsunamis included wave periods too short (~1–2 min) to be well captured by tide gauge running at the typical sampling intervals of 1 min. Whether the sea level fluctuations (periods of ~6 min) captured by the Pantoloan tide gauge have a different origin than the shorter-period waves observed in video footage, for example, from a combination of landslide and tectonic sources, or simply reflect an aliased version of shorter-period tsunami waves cannot be confirmed.

3. The Role of Coastal Landslides in the Palu Tsunamis

Our simulated tsunamis based on initial conditions from the fault slip models published to date (ie., Socquet et al., 2019; USGS, 2018) fail to fully explain the surveyed runups (Fritz et al., 2018) and cannot predict the tsunami waveforms inferred from our analysis of video footage (Figure 2; see methods for tsunami modeling). Aside from Dupa, where both slip models predict the video observations reasonably well, the inferred phases and amplitudes at the other five sites cannot be reproduced from these slip models (Figure 2b). This may be explained with three scenarios: (1) Slip models fail to predict the actual seafloor displacements beneath Palu Bay, which is possible owing to data limitations and uncertainties in both offshore fault geometry and seafloor mechanical properties; (2) our tsunami models fail to reproduce particular aspects of unusually short-period waves; and/or (3) additional nontectonic sources, such as submarine landslides triggered by strong seismic shaking (Bao et al., 2019), contributed to tsunami generation.

Widespread onshore landslides were triggered by the Palu earthquake (Petley, 2018; Sassa & Takagawa, 2019), and submarine slope failures may be a plausible mechanism to explain the additional sources required by the reconstructed tsunami waveforms. Indeed, the tsunamis observed in the tide gauge record at Mamuju, located ~200 km south of the Palu Bay (Figures 1a and 1c), may have been very likely triggered by landslides outside the bay. There, the local tide gauge station recorded tsunami amplitudes of up to 6 cm arriving 25 min after the mainshock. Based on simulated tsunami travel times, the source must be within 100 km of Mamuju, and thus is incompatible with the timing of a source near Palu Bay and the fault rupture (Figure 1a). Heidarzadeh et al. (2019) ascribed the Mamuju tsunami to the earthquake by proposing a 45-min delay on the tide gauge station clock to fit modeled and predicted waveforms; however, this assessment seems unlikely for two reasons. First, the official cancellation of the tsunami alert, 34 min after the earthquake, was decided based on the 6-cm small tsunamis recorded by the Mamuju tide gauge station (Hoffmann et al., 2018). And second, such a clock error would also imply a delay between the tides of Mamuju and Pantoloan (Figure S7), which does not seem to be the case (Informasi Geospasial, 2018b). Therefore, shaking-triggered landslides are the most reasonable source for the tsunamis observed at Mamuju, which is interesting since seismic shaking in this area (enclosed by the 25-min isoline in Figure 1a) is expected to be significantly less intense than in the area surrounding the fault zone, especially within Palu Bay.

To explore the possible role of submarine landslides as tsunami sources within Palu Bay, we analyzed video footage and satellite images to determine likely source regions. A detailed comparison of pre-and post-earthquake satellite imagery revealed evidence of shoreline retreat at 18 sites around Palu Bay of distances from 10 to 120 m (Figures 2 and S8). Interestingly, all cases occurred along coastal plains adjacent to fluvial and alluvial fan deltas (Figure S8) and, therefore, may be interpreted as the surface expressions of submarine failures of these landforms. Deltas, formed from unconsolidated material, are very sensitive to failure by an external trigger such as seismic shaking (Girardclos et al., 2007; Hasiotis et al., 2006; Hilbe & Anselmetti, 2014; Leithold et al., 2018). Furthermore, the potential for delta failures to generate significant tsunamis during strong shaking events (Vanneste et al., 2018) has been documented at sites with diverse climatic conditions, such as Alaska (USA; Field et al., 1982; Parsons et al., 2014) and Haiti (Hornbach et al., 2010).

Evidence for tsunamis induced by delta failures during the Palu event is supported by video footage. Four extraordinary amateur videos, taken from a plane, a moored boat and from high ground captured the initiation and/or early formation of 7 tsunamis along the west coast of the bay (Figure 3 and videos 38–41). Strikingly, all of these came from areas where delta landforms failed during the Palu earthquake (Figures 2a and S8). However, based on their small sizes and late timing, they seem unlikely to be the complementary sources required to explain all the tsunami observations around Palu Bay. In order to explore whether similar sources occurred elsewhere in the bay, we interviewed Ricoseta Mafella, the aircraft pilot who collected video 38. Although he noticed that these sea level phenomena were only present along the western coast of the bay, he only had a clear view of the eastern flank about 3 min after the mainshock when he turned "left" (west). This time, however, may be too late given the nearly instantaneous occurrence of the Palu tsunamis and therefore, tsunamis triggered by submarine landslides along the eastern shore of the bay cannot be ruled out. Indeed, a video recorded at Taipa (Figure 2a) captured a large tsunami wave coming from the northeast coast of the bay (video 31 and Figures 3e and 3h). Although not as evident as the landslide tsunamis originating along the west coast, the steepness and seaward traveling direction of the wave seen in
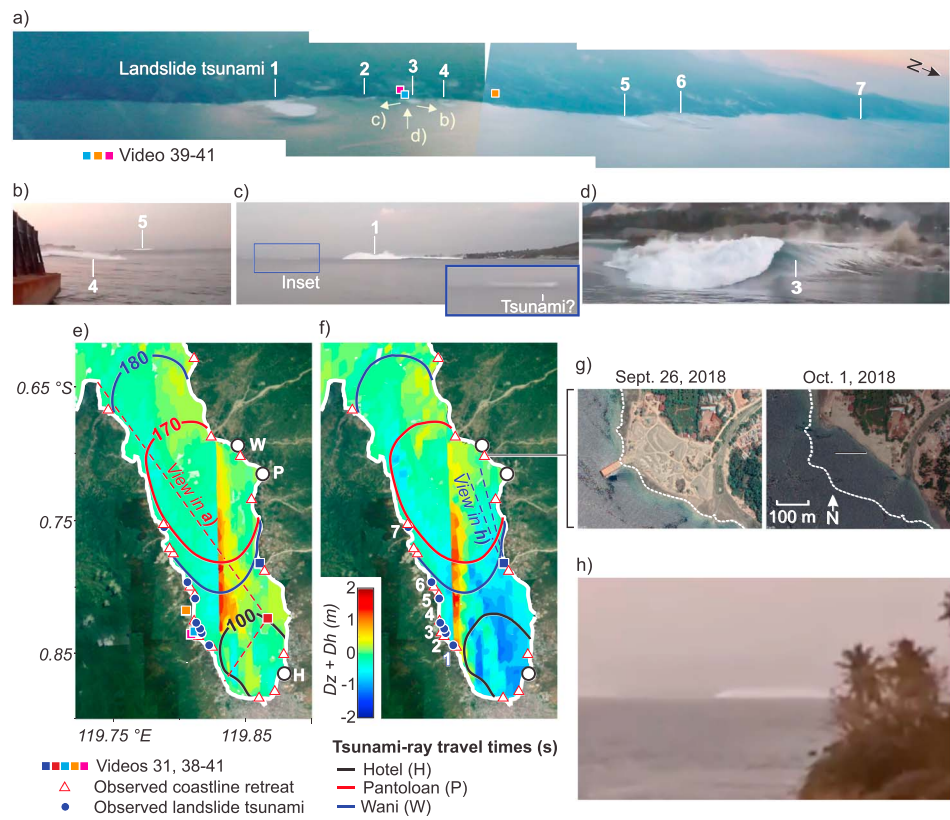
Figure 3. Examples of tsunamis interpreted to have been associated with submarine landslides and probable landslide locations inferred from a combined analysis of pre-and post earthquake satellite imagery and video footage. (a) Seven point-source sea level perturbations along the western coast of Palu Bay captured at ~1,000-m elevation by aircraft pilot Ricosseta Mafella (video 38). In the vicinity of landslide tsunami 3, a boat captured the tsunamis shown in (b)–(d) (video 39). Inset in (c) shows an additional sea level perturbation which could have been the first large wave to hit Palu (see text). (e) and (f) Tsunami-ray travel times (in seconds) from Wani, Pantoloan, and KN Hotel superimposed on vertical displacements of the sea surface due to vertical coseismic deformation (Dz) and the bathymetry effect (Dh; Tanioka & Satake, 1996), predicted by the fault slip models (Socquet et al., 2019; USGS, 2018, respectively). (g) Pre-and post-earthquake satellite images showing the shoreline between Pantoloan and Wani. Note pronounced retreat of the deltaic coastal plain. (h) Snapshot of video 31 when filming toward the north of the bay where a tsunami wave propagates seaward (see video 31).

the video seem more consistent with a localized source near the coastline than one produced by the earthquake faulting beneath the bay.

The precise arrival times estimated at Wani, Pantoloan, and the KN Hotel can be used to locate probable individual landslides sources. Figures 3e and 3f show the possible source regions predicted from backward tsunami-ray tracing from the video-inferred arrival times (methods), superimposed on the seafloor displacement patterns predicted by rupture models (Socquet et al., 2019; USGS, 2018) and coastline retreats inferred by satellite imagery (Figure S8). These isolines cross the areas of largest seafloor displacement and include multiple locations of coastline retreat, suggesting that the rapid arrival times at these three locations can be explained either by fault slip or by delta failures associated with such coastline retreats. However, the tsunami amplitudes reconstructed at these locations are 3 times greater than those predicted by tsunami simulations based on seafloor displacements (Figure 2b), and therefore, fault slip alone fails to fully explain the video-observed tsunamis at Wani, Pantoloan, and KN Hotel. Although bathymetric surveys are needed to address the occurrence of delta failures near the locations of coastline retreat, they are plausible candidates for localized, complementary tsunami sources. Particularly intriguing is the region between Pantoloan and Wani (Figure 3g), where we mapped the largest coastline retreat in Palu Bay (up to ~120 m). Failure of a delta front there would produce an immediate sea level drawdown followed by rapid tsunami inundation, as has been predicted by numerical simulations of other tsunamis (Watts et al., 2005) and reported by eyewitnesses to the tsunamis produced by delta

failures triggered by the 2010 Haiti earthquake (Hornbach et al., 2010). Interestingly, such a sea level response was inferred from video footage and eyewitness reports immediately north (Wani) and south (Pantoloan) of this pronounced coastline retreat (Text S2 and S3 and video 11). Although plausible, whether or not this was the source for the large wave propagating seaward from this part of the bay (Figures 3e and 3h), as seen in video 31, cannot be confirmed with the available data.

4. Concluding Remarks and Future Work

Our video-based analysis indicates that although the Palu earthquake was produced by predominantly horizontal fault slip, it generated devastating tsunamis reaching widespread coastal areas of Palu Bay nearly instantaneously, within tens of seconds after the end of seismic shaking. Shallow slip extending to the surface combined with the steep bathymetry of the long and narrow Palu Bay likely contributed to the large runups observed around the bay, which were further enhanced by the high tide (~1 m above MSL) at the time of the tsunami (Figure 1b). However, we note that tsunami simulations from existing fault slip models are not sufficient to reproduce the runup heights measured in field surveys, and cannot explain the spatial and temporal patterns inferred from the video-derived tsunami waveforms and local tide gauges. Unless these fault models underestimate the actual dip-slip component beneath Palu Bay, additional non-tectonic tsunami sources are likely to have contributed to tsunami generation. In this case, submarine landslides triggered by delta failures along the bay are plausible candidates for such supplementary sources, as suggested by locations of observed coastline retreat, video footage and tsunami-ray travel time simulations.

Our results provide valuable data and guidance for future efforts aimed at understanding the sources of the Palu tsunamis. Our inferred tsunami waveforms (available in the supporting information) may be used to test future fault slip models with improved offshore resolution and guide dedicated modeling experiments of tsunamis generated by a combination of submarine landslides and coseismic seafloor deformation. Additionally, our satellite imagery results can guide detailed bathymetric surveys where delta failures, potentially acting as tsunami sources, may have occurred. Based on our video analysis, we emphasize that future studies should use tsunami modeling strategies capable of simulating the generation, propagation and runup of unusually short-period tsunamis such as those observed. Finally, we highlight that the 1-min sampling interval of the Pantoloan tide gauge record did not reliably capture the damaging short-period features of the Palu tsunamis inferred from our analysis of CCTV footage captured in the vicinity of the station. This instrumental limitation, revealed by our analysis of video footage, has critical implications for tsunami early warning systems based on real-time sea level observations along coasts adjacent to diverse tectonic settings.

The tragic Palu story highlights several important lessons to be considered in areas with similar geomorphic and tectonic settings potentially exposed to tsunami hazards. The main lesson is that tsunami risk needs to be assessed locally; hazard assessments must consider all reasonable sources of tsunami generation based on the local tectonic setting and including areas of potential landslides. Also, because inundation and damage caused by short period waves can be quite different than those caused by longer period waves in a limited coastal inundation zone, a locally defined spectrum of wave periods must be considered, and according modeling strategies and bathymetric data must be used. Local infrastructure and urban design should consider this and other local aspects of tsunami hazards. The Palu tsunamis demonstrated that damaging waves may arrive within a few minutes after the seismic shaking, and therefore, escape routes must be appropriately located and oriented to allow timely self-evacuations, and if not possible, vertical evacuation shelters must be implemented.

Our waveform reconstructions from video footage complement previous video-based approaches (e.g., Fritz et al., 2006, 2012; Koshimura & Hayashi, 2012) aimed to better understand tsunami phenomena. We encourage the increased scientific use of tsunami videos shared on social media platforms that provide valuable constraints for scientific studies and help guide tsunami hazard mitigation efforts and focused post-tsunami surveys.

References

Associated Press (2018). Indonesia Earthquake Ship. http://www.aparchive.com/metadata/youtube/abf7ff674bfc102aec5cdf7b7a959423
Bao, H., Ampuero, J. P., Meng, L., Fielding, E. J., Liang, C., Milliner, C. W., et al. (2019). Early and persistent supershear rupture of the 2018 magnitude 7.5 Palu earthquake. *Nature Geoscience*, *12*, 200–205. https://doi.org/10.1038/s41561-018-0297-z

Bellier, O., Sébrier, M., Beaudouin, T., Villeneuve, M., Braucher, R., Bourlès, D., et al. (2001). High slip rate for a low seismicity along the Palu-Koro active fault in central Sulawesi (Indonesia). *Terra Nova*, *13*, 463–470. https://doi.org/10.1046/j.1365-3121.2001.00382.x

Chicago Tribune (2018). Crew members recount terror of tsunami that dumped 208-foot ferry in Indonesian village. https://www.chicagotribune.com/news/nationworld/ct-indonesia-tsunami-ferry-ashore-20181004-story.html

Cienfuegos, R., Catalán, P. A., Urrutia, A., Benavente, R., Aránguiz, R., & González, G. (2018). What can we do to forecast tsunami hazards in the near field given large epistemic uncertainty in rapid seismic source inversions? *Geophysical Research Letters*, *45*, 4944–4955. https://doi.org/10.1029/2018GL076998

Digital Globe (2018). Open Data program, Indonesia earthquake and Tsunami. https://www.digitalglobe.com/opendata/indonesia-earthquake-tsunami/post-event

Field, M. E., Gardner, J. V., Jennings, A. E., & Edwards, B. D. (1982). Earthquake-induced sediment failures on a 0.25° slope, Klamath River delta, California. *Geology*, *10*(10), 542–546. https://doi.org/10.1130/0091-7613(1982)10<542:ESFOAS>2.0.CO;2

Fritz, H. M., Borrero, J. C., Synolakis, C. E., & Yoo, J. (2006). 2004 Indian Ocean tsunami flow velocity measurements from survivor videos. *Geophysical Research Letters*, *33*, L24605. https://doi.org/10.1029/2006GL026784

Fritz, H. M., Phillips, D. A., Okayasu, A., Shimozono, T., Liu, H., Mohammed, F., et al. (2012). The 2011 Japan tsunami current velocity measurements from survivor videos at Kesennuma Bay using LiDAR. *Geophysical Research Letters*, *39*, L00G23. https://doi.org/10.1029/2011GL050686

Fritz, H. M., Synolakis, C., Kalligeris, N., Skanavis, V., Santoso, F., Rizal, M., et al. (2018). Field survey of the 28 September 2018 Sulawesi tsunami. *Eos, Transactions of the American Geophysical Union*, *99*, 53.

Girardclos, S., Schmidt, O. T., Sturm, M., Ariztegui, D., Pugin, A., & Anselmetti, F. S. (2007). The 1996 AD delta collapse and large turbidite in Lake Brienz. *Marine Geology*, *241*(1-4), 137–154. https://doi.org/10.1016/j.margeo.2007.03.011

Hasiotis, T., Charalampakis, M., Stefatos, A., Papatheodorou, G., & Ferentinos, G. (2006). Fan delta development and processes offshore a seasonal river in a seismically active region, NW Gulf of Corinth. *Geo-Marine Letters*, *26*(4), 199–211. https://doi.org/10.1007/s00367-006-0020-8

Heidarzadeh, M., Muhari, A., & Wijanarto, A. B. (2019). Insights on the source of the 28 September 2018 Sulawesi tsunami, Indonesia based on spectral analyses and numerical simulations. *Pure and Applied Geophysics*, *176*(1), 25–43. https://doi.org/10.1007/s00024-018-2065-9

Hilbe, M., & Anselmetti, F. S. (2014). Signatures of slope failures and river-delta collapses in a perialpine lake (Lake Lucerne, Switzerland). *Sedimentology*, *61*(7), 1883–1907. https://doi.org/10.1111/sed.12120

Hoffmann T., Triyono R., Weniza, A., Heryandoko, N., Daniarsyad, G., Karyono, A., et al. (2018). The 2018 Mw 7.5 Sulawesi Indonesia earthquake: The immediate response of the InaTEWS Warning Centre at BMKG and related operational issues. Paper presented at the Fall Meeting, AGU, Washington DC, December 10-14, 2018.

Hornbach, M. J., Braudy, N., Briggs, R. W., Cormier, M.-H., Davis, M. B., Diebold, J. B., et al. (2010). High tsunami frequency as a result of combined strike-slip faulting and coastal landslides. *Nature Geoscience*, *3*(11), 783. https://doi.org/10.1038/ngeo975

Imamura, F., Synolakis, C. E., Gica, E., Titov, V., Listanco, E., & Lee, H. J. (1995). Field survey of the 1994 Mindoro Island, Philippines tsunami. *Pure and Applied Geophysics*, *144*(3-4), 875–890. https://doi.org/10.1007/BF00874399

Informasi Geospasial (2018a). Contour map of Palu Bay, Retrieved from https://cloud.big.go.id. Accessed 15 Oct. 2018.

Informasi Geospasial (2018b). Real time tidal observation, Retrieved from http://tides.big.go.id:8888/dash/. Accessed 28 Feb. 2019.

Katili, J. A. (1970). Large transcurrent faults in Southeast Asia with special reference to Indonesia. *Geologische Rundschau*, *59*(2), 581–600. https://doi.org/10.1007/BF01823809

Koshimura, S., & Hayashi, S. (2012). Tsunami flow measurement using the video recorded during the 2011 Tohoku tsunami attack. In *2012 IEEE International Geoscience and Remote Sensing Symposium* (pp. 6693–6696). Munich, Germany: IEEE. https://doi.org/10.1109/IGARSS.2012.6352063

Leithold, E. L., Wegmann, K. W., Bohnenstiehl, D. R., Smith, S. G., Noren, A., & O'Grady, R. (2018). Slope failures within and upstream of Lake Quinault, Washington, as uneven responses to Holocene earthquakes along the Cascadia subduction zone. *Quaternary Research*, *89*(1), 178–200. https://doi.org/10.1017/qua.2017.96

Mori, N., Takahashi, T., Yasuda, T., & Yanagisawa, H. (2011). Survey of 2011 Tohoku earthquake tsunami inundation and run-up. *Geophysical Research Letters*, *38*, L00G14. https://doi.org/10.1029/2011GL049210

Muhari, A., Imamura, F., Arikawa, T., Hakim, A. R., & Afriyanto, B. (2018). Solving the puzzle of the September 2018 pale, Indonesia, tsunami mystery: Clues from the tsunami waveform and the initial field survey data. *Journal of Disaster Research*, *13*, sc20181108.

Omira, R., Dogan, G. G., Hidayat, R., Husrin, S., Prasetya, G., Annunziato, A., et al. (2019). The September 28th, 2018, tsunami in Palu-Sulawesi, Indonesia: A post-event field survey. *Pure and Applied Geophysics*, 1–17.

Parsons, T., Geist, E. L., Ryan, H. F., Lee, H. J., Haeussler, P. J., Lynett, P., et al. (2014). Source and progression of a submarine landslide and tsunami: The 1964 Great Alaska earthquake at Valdez. *Journal of Geophysical Research: Solid Earth*, *119*, 8502–8516. https://doi.org/10.1002/2014JB011514

Petley, D. (2018). Landslide tsunamis from the Sulawesi earthquake. The Landslide Blog, 19 October 2018. https://blogs.agu.org/landslideblog/2018/10/19/landslide-tsunamis-sulawesi-earthquake

Prasetya, G. S., De Lange, W. P., & Healy, T. R. (2001). The Makassar Strait tsunamigenic region, Indonesia. *Natural Hazards*, *24*(3), 295–307. https://doi.org/10.1023/A:1012297413280

Sassa, S., & Takagawa, T. (2019). Liquefied gravity flow-induced tsunami: First evidence and comparison from the 2018 Indonesia Sulawesi earthquake and tsunami disasters. *Landslides*, *16*(1), 195–200. https://doi.org/10.1007/s10346-018-1114-x

Satake, K., Fujii, Y., Harada, T., & Namegaya, Y. (2013). Time and space distribution of coseismic slip of the 2011 Tohoku earthquake as inferred from tsunami waveform data. *Bulletin of the Seismological Society of America*, *103*(2B), 1473–1492. https://doi.org/10.1785/0120120122

Socquet, A., Hollingsworth, J., Pathier, E., & Bouchon, M. (2019). Evidence of supershear during the 2018 magnitude 7.5 Palu earthquake from space geodesy. *Nature Geoscience*, *12*(3), 192–199. https://doi.org/10.1038/s41561-018-0296-0

Socquet, A., Simons, W., Vigny, C., McCaffrey, R., Subarya, C., Sarsito, D., et al. (2006). Microblock rotations and fault coupling in SE Asia triple junction (Sulawesi, Indonesia) from GPS and earthquake slip vector data. *Journal of Geophysical Research*, *111*, B08409. https://doi.org/10.1029/2005JB003963

Soloviev, S. L., & Go, C. N. (1974). *A Catalogue of Tsunamis on the Western Shore of the Pacific Ocean*. Moscow: Nauka Publishing House.

Tanioka, Y., & Satake, K. (1996). Tsunami generation by horizontal displacement of ocean bottom. *Geophysical Research Letters*, *23*(8), 861–864. https://doi.org/10.1029/96GL00736

U.S. Geological Survey (2018). M 7.5-70km N of Palu, Indonesia, https://earthquake.usgs.gov/earthquakes/eventpage/us1000h3p4/finite-fault

Vanneste, K., Wils, K., & Van Daele, M. (2018). Probabilistic evaluation of fault sources based on paleoseismic evidence from mass-transport deposits: the example of Aysén Fjord, Chile. *Journal of Geophysical Research: Solid Earth*, *123*, 9842–9865. https://doi.org/10.1029/2018JB016289

Walpersdorf, A., Vigny, C., Manurung, P., Subarya, C., & Sutisna, S. (1998). Determining the Sula block kinematics in the triple junction area in Indonesia by GPS. *Geophysical Journal International*, *135*(2), 351–361. https://doi.org/10.1046/j.1365-246X.1998.00641.x

Ward, S. (2011). Tsunami. In H. K. Gupta (Ed.), *Encyclopedia of Solid Earth Geophysics*, *Encyclopedia of Earth Sciences Series* (pp. 1473–1493). Dordrecht: Springer. https://doi.org/10.1007/978-90-481-8702-7

Watkinson, I. M., & Hall, R. (2017). Fault systems of the eastern Indonesian triple junction: evaluation of Quaternary activity and implications for seismic hazards. *Geological Society, London, Special Publications*, *441*(1), 71–120. https://doi.org/10.1144/SP441.8

Watkinson, I. M., Hall, R., Cottam, M. A., Sevastjanova, I., Suggate, S., Gunawan, I., et al. (2012). New insights into the geological evolution of Eastern Indonesia from recent research projects by the SE Asia Research Group. *Berita Sedimentologi*, *23*, 21–27.

Watts, P., Grilli, S. T., Tappin, D. R., & Fryer, G. J. (2005). Tsunami generation by submarine mass failure. II: Predictive equations and case studies. *Journal of Waterway, Port, Coastal, and Ocean Engineering*, *131*(6), 298–310.

References From the Supporting Information

Okada, Y. (1985). Surface deformation due to shear and tensile faults in a half-space. *Bulletin of the Seismological Society of America*, *75*(4), 1135–1154.

Pawlowicz, R., Beardsley, B., & Lentz, S. (2002). Classical tidal harmonic analysis including error estimates in MATLAB using T_TIDE. *Computers & Geosciences*, *28*(8), 929–937. https://doi.org/10.1016/S0098-3004(02)00013-4

Torrence, C., & Compo, G. P. (1998). A practical guide to wavelet analysis. *Bulletin of the American Meteorological Society*, *79*(1), 61–78. https://doi.org/10.1175/1520-0477(1998)079<0061:APGTWA>2.0.CO;2

Wang, X. (2009). User manual for COMCOT version 1.7 (first draft). Cornel University, 65.

Nearly-instantaneous tsunamis following the Mw 7.5 2018 Palu earthquake

Matías Carvajal[1,2], Cristian Araya-Cornejo[3], Ignacio Sepúlveda[4], Daniel Melnick[2,5], Jennifer S. Haase[4]

1Departamento de Ciencias de la Tierra, Universidad de Concepción, Concepción, Chile

2Millennium Nucleus The Seismic Cycle Along Subduction Zones, Chile

3Observatorio de Gestión de Riesgo de Desastres, Universidad Bernardo O'Higgins, Santiago, Chile.

4Institute of Geophysics and Planetary Physics, Scripps Institution of Oceanography, UC San Diego

5Instituto de Ciencias de la Tierra, Universidad Austral de Chile, Valdivia, Chile

Contents of this file

Methods for tsunami simulation
Text S1 to S3
Figures S1 to S8
Table S1 and S2

Additional Supporting Information (Files uploaded separately)

Captions for Dataset S1 and S2

Introduction

This supporting information includes (1) the methods used for numerical modeling experiments and for waveform reconstruction (Text S1), (2) complementary descriptions of the tsunamis at the different studied sites (Text S2-4 and Figures S1-4), (3) the inferred tsunami inundation limit around Palu Bay (Figure S5), (4) time-frequency analysis and results for the Pantoloan and Mamuju tide gauge records (Figure S6), (5) tide gauge waveforms at Mamuju and Pantoloan that support the idea that the tide station of Mamuju does not have an error in its clock, as previously suggested, (6) Satellite imagery observations and analysis for coastal retreats around Palu Bay (Figure S8), and (7) the repository location of the video data set used in this study (Table S1) and a summary of those used for waveform reconstruction. Datasets S1 and S2 are provided in separate files.

Methods for numerical modeling experiments.

<u>Tsunami simulations</u>

Tsunami waveforms and runup were predicted from the existing fault slip models of the Palu earthquake (Socquet et al. 2019; USGS 2018) through tsunami modeling techniques. The initial tsunami conditions were inferred by the vertical seafloor deformations due to earthquake faulting (Okada 1985) and the bathymetry effect produced by horizontal displacements (Tanioka and Satake 1996). Tsunami propagation and inundation were computed by using a finite-difference method on modern bathymetry for Palu Bay. We employed the tsunami propagation model COMCOT, which solves the non-linear shallow water wave equations (NLSWE) in a leap frog finite difference scheme (Wang 2009). We used a one-level grid domain with ~23 m spatial resolution, built from the official bathymetry data of the agency Badan Informasi Geospasial (Informasi Geospasial 2018; http://www.big.go.id) from the most comprehensive survey done in 2014, verified with local nautical charts of Sulawesi from the hydrographic Office of the UK at 1:200,000 scale. We further simulate the bottom friction dissipation using the quadratic Manning's law and a coefficient of 0.03 s·m$^{-1/3}$ (Bricker et al. 2015). Radiating boundary conditions for the open boundaries (i.e. mouth of the bay) and moving boundaries at the coast were used to simulate the wave runup. A 1-sec computational time step was set to satisfy the Courant-Friedrichs-Lewy stability condition. All tsunami simulations were run for 30 min. The reference water level for all simulations was set to ~1 m above mean sea level, according to the local water level estimated at the time of the earthquake (Fig. 1B).

<u>Tsunami ray travel times</u>

Tsunami travel times for Wani, Pantoloan, KN Hotel and Mamuju were calculated by backward propagating point sources from these locations (Fig. 1A and 3E,F). Propagation calculations were based on the NLSWE and considered a similar approach to that described above. The tsunami-ray travel times for Wani are based on the inundation phase observed in videos rather than on the earlier initial sea-level decrease reported by eyewitnesses. Therefore, the range to the source region predicted for Wani is likely overestimated.

<u>Tide level prediction</u>

Sea level at the moment of the earthquake was predicted from 36 days of tidal observations by the Pantoloan tide gauge station. Tidal constituents were determined by a harmonic analysis (using the least-squares method), which were then used for the predictions. To this end, we used the T-Tide MATLAB toolbox (Pawlowicz et al. 2002).

Text S1

Tsunami waveform reconstructions constitute the key analysis of this study. The compiled videos provide relevant information about arrival times, wave periods and amplitudes in many coastal locations of Palu bay. Overall, tsunami waveform reconstruction was possible at 6 sites: Palu city, the KN Hotel, Talise, Dupa, Pantoloan and Wani (Fig. 2A). The water level was estimated at 2 second intervals from the location of individual pixels in the image and stored with the video time of the image. The video time was then referenced to the time of shaking observed in the video. For waveform reconstruction we extracted the apparent sea level change relative to still water level observed at the shoreline (dry/wet contrast) in earlier video image frames, which is assumed to be the 1 m tidal level at the moment of the tsunami (Figure 1B). At Dupa, for example, the video began with an apparent sea level retreat of 0.5 m. The initial point of the waveform in Figure 2 is, therefore, the 1 m tidal level minus 0.5 m which equals 0.5 m above mean sea level. For dimensional references we used Google Earth and Google Street views as well as local photographs and videos found in the internet.

Arrival time estimations were possible only at those sites where continuous video recordings show both the seismic shaking and the tsunami arrival. In these cases, the arrival times were calculated by considering the time span between seismic shaking and impact of evident tsunami waves, which was clear in most of the cases. The arrival times were satisfactorily estimated at KN Hotel, Talise, Pantoloan and Wani. The initiation of the ground shaking at the site and the earthquake origin time can be on the order of 10 s, given propagation of seismic waves from the epicenter located ~64 km from Palu Bay at typical S-wave velocities. We neglect this difference and assign an error in the absolute arrival time of 10 seconds. The relative error of the arrival times among the 5 sites is less, given that they are relatively close together (within a radius of ~20 km). At Palu city and Dupa, we could not find videos that provided continuous recordings of both shaking and tsunami impact, and thus arrival times could not be precisely estimated. However, in Figure 2a we provide rough estimates based on the human behavior inferred form the videos. In particular, the videos collected at Dupa (video 14) and Palu city (videos 15 and 16) show people in a state of panic, a situation expected within the first few minutes following strong earthquakes. In these cases, we estimated time spans of 1 and 2 minutes between the earthquake and the beginning of videos at Dupa and Palu city, respectively. Thus, we estimated arrival times relative to the earthquake at Dupa and Palu city, by considering these time spans and the arrival times relative to the video onsets. Although we acknowledge that the arrival time estimates at these locations may differ by up to 120 s from actual values, these errors do not affect the conclusions reached in our study.

Wave periods at Palu city and Pantoloan were estimated by a similar approach. At Palu city we temporally synchronized seven videos that recorded the tsunamis from different sites (see main text). By combining the synchronized videos, the time span between incoming waves (ie., wave periods) can be easily estimated. The wave periods at Pantoloan were estimated from one CCTV video (video 11) that captured the vertical movements of a moored ship (a manual acceleration of the video is recommended to see more clearly the up and down movements of the ship). We assign an error of 2 s to the periods estimated from the videos.

Wave amplitudes are more difficult to estimate. In general, we estimated wave amplitudes by comparing the heights reached by the tsunamis of the videos with Google Earth imaging, Google Street views, local photographs and videos of the locations prior the earthquake. For dimensional references we used cars, buildings, people, walls and other elements of roughly known dimensions. For the case of Pantoloan, where tsunami parameters were estimated by the vertical movements of the KM MERATUS KENDARI 1 container ship (berthed during the earthquake and tsunami at the northern wharf of the Pantoloan port), we used the actual dimensions of that ship, which were obtained from the International Maritime Organization (IMO) number of the container vessel, which is a unique identifier for ships (Text S4 and Figure S3e-j). To the reconstructed amplitudes (vertical distance between crest or trough to still water level) at Palu city and KN Hotel an uncertainty of 20% is realistic based on the typical ability to distinguish the maximum height relative to the objects of standard size observed in the videos. Assigning amplitude values and errors at the other locations is more difficult, and in these cases we estimated conservative (minimum) values of amplitude. Specifically, for the waveforms at Pantoloan and Wani actual amplitudes may have been much greater (> 1 m higher) than the minimum values reported in our reconstructions, but quantitative errors cannot be assigned with confidence. At Dupa and Talise the videos did not capture the inundation, and therefore the amplitude uncertainty cannot be assessed. However, the key observation at these sites is the arrival time of the leading wave and its initial negative polarity. Despite the fact that the amplitudes shown in our video-inferred waveforms (Fig. 2A) may contain large uncertainties,

specifically those at Talise, Dupa, Pantoloan and Wani, they provide rough values that can be used as a reference for other studies attempting to assess the sources for the Palu tsunamis.

Text S2

The CCTV cameras of the Kampung Nelayan (KN) Hotel, located in the southeast coast of Palu Bay, revealed fundamental information about the Palu tsunamis. The KN Hotel had at least 7 cameras operating when the earthquake and tsunamis struck, from which 6 recorded the earthquake and the tsunami. The configuration of the CCTV array provided wide coverage of the area that included almost 150 m of coastline (videos 1-3). Figure S1 shows the visual field of each camera.

Shockingly, the tsunami here arrived 101 seconds after the earthquake shaking. Videos 1, 2 and 3, which had a clear view of the coastline, recorded the shaking, which began at 17:59:45 (camera time), and large tsunami inundation beginning at 18:01:26. Also clear from video 3 is an initial positive tsunami sea-level elevation, which in a matter of seconds inundated the entire area where the hotel is located, as shown by all 6 videos. By combining the videos and comparing with Google Earth and Google Street views we estimate a flow depth of about 2-3 m inundating at about 4-5 m/s for this initial inundation.

Another hazardous feature of the initial tsunamis that affected the KN Hotel was their multi-directional impact. Videos 1 and 2 show initial inundation coming from the north-northeast. Contrastingly, videos 3, 4 and 6 show the incoming waves coming initially from the north-northwest direction. The north-northwest direction consequently produced oblique inundation on land, and a perpendicular impact on the evacuation road (Fig. S1c,d,e). Unfortunately, the local inundation line inferred from satellite imagery was landward and nearly parallel to the evacuation road, and therefore, evacuation may have not been fully successful (Fig. S1).
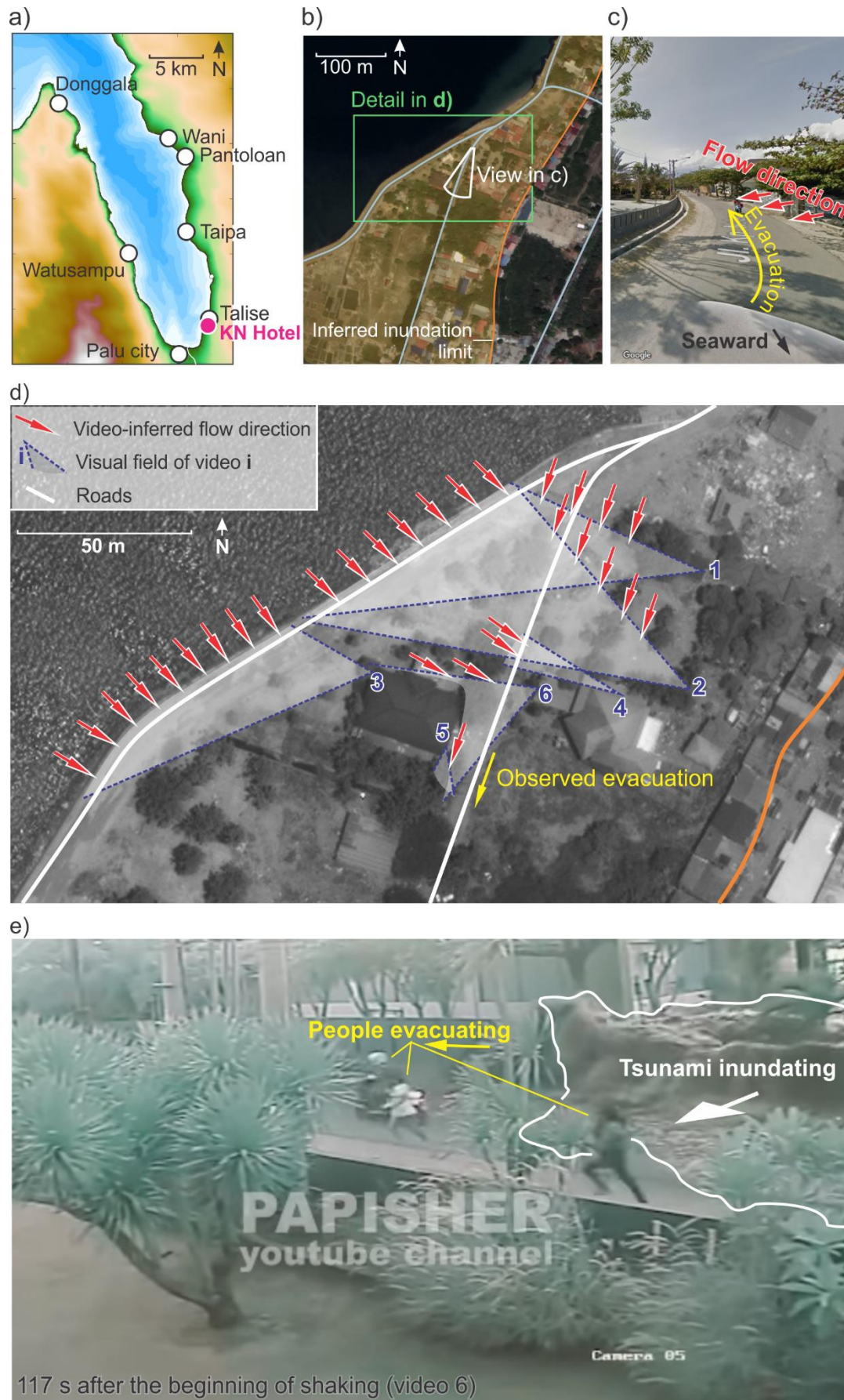
Text S3

Two videos that rapidly caused widespread reaction on social media platforms were taken in a house at Wani, about 20 km north of the KN Hotel. After an exhaustive online search, we located the house on the map, which is shown in Figure S2. The house is 150 m landward from the coastline and about 20 m seaward from the local inundation limit that we inferred from satellite imagery (Fig. S5). The videos show (videos 7-8), from two different angles of CCTV cameras, children present in the front yard of the house when suddenly, at 18:02:54 (camera time), strong shaking begins. At 18:06:28, 214 seconds later, a tsunami inundates the front yard. Unlike the story at the KN Hotel, the timely exit of the children from the video scene, combined with the favorable orientation of the evacuation road very likely indicates a successful evacuation even for such a fast arriving tsunami (Fig. S2).

Two more videos complement the observations at the house in Wani (videos 9-10). The videos were taken from a passenger ship (video 9) and a fishing boat (video 10), at the locations shown in Figure S2. Video 9, taken onboard the Sabuk Nusantara 39 Passenger Ship, shows an initial landward flooding followed by a water retreat. It is clear, however, that the video starts after the largest inundation at Wani, as suggested by the severe destruction already present in the scene and also because the ship is already stranded on the wharf. Based on the tsunami inundation at the house, we believe the video was taken over 3 min after the earthquake. This interpretation is consistent with testimonies from crewmembers of the ship. They reported a ~7 m decrease in the sea level immediately after the earthquake, followed 3-5

min later, by a ~15 m large wave that stranded them over the wharf (Press 2018; Tribune 2018). Note that, for an eyewitness, a wave of 15 m height arriving after a 7 m water retreat implies a tsunami of 8 m amplitude relative to initial sea level. Although we cannot confirm such a large tsunami, the amplitude there had to be at least 5 m to "smoothly" (as the crewmembers recall) move the ship over the wharf. This estimate considers the ~3 m average draft of that ship (IMO 9712802) and a minimum wharf height of 2 m (see Fig. S2b for reference). The video taken onboard the fishing ship (video 10) provides no quantitative information about the tsunamis at Wani. However, it complements the visual field of video 9 and contributes confidence in the geolocation and orientation information.

Text S4

Tsunami waves observed at Pantoloan port by a CCTV camera challenge the only instrumental record inside Palu Bay. A CCTV video (video 11), unfortunately of poor resolution, recorded the shaking and subsequent tsunami waves (Fig. S3). The video also captures the moment when the container crane collapses due to the strong shaking (Figure S3). The sea-level behavior is inferred here by the vertical movements of the KM Meratus Kendari 1, a 120-m long container ship that was berthed at the north wharf when the earthquake and tsunami hit. A manual acceleration of the video is recommended to see more clearly the vertical movements of the ship. Using the ship's dimensions as a reference (Fig. S3j), we infer an initial water retreat over 2 m beginning ~3 min after the end of seismic shaking followed by a rapid sea-level rise of at least ~4 m (Fig. S3e-i). The inferred tsunami waveform is shown in Figure 2B. Interestingly, the waveform at this initial time was not observed by the tide gauge station located at the same port (Fig. S3). Additional short video segments immediately after the earthquake, as well as after the initial tsunami waves caught by the CCTV camera, were captured by a crewmember onboard the ship (video 12). Although we could not retrieve additional information from this video, it supports the CCTV video observations, because it does not show an immediate water drawdown after the earthquake as inferred at other places, such as Wani, Dupa and Talise.

a)

b) Detail in d)
View in c)
Inferred inundation limit

c) Flow direction
Evacuation
Seaward

d)
- Video-inferred flow direction
- **i** Visual field of video **i**
- Roads

50 m   N

1
2
3
6
4
5
Observed evacuation

e)
People evacuating
Tsunami inundating

PAPISHER youtube channel

Camera 05

117 s after the beginning of shaking (video 6)

6

Figure S1. Video analyses at the KN Hotel. a) Map of Palu Bay and location of the KN Hotel. b) Satellite image of the KN Hotel and its surroundings. The inundated area as inferred from satellite imagery is shown by the orange colored region. c) Google Street view of the road used for evacuation. Red arrows indicate a nearly-perpendicular tsunami impact on the evacuation road. d) Array of CCTV cameras, showing the field view of each. The numbering corresponds to the video code of Table S1. The orange line indicates the inundation limit as inferred from satellite imagery. e) Snapshot of video 6 showing the beginning of inundation on the evacuation road.

a)

b)

Location of videos
▽ 7-8 (House)　▽ 9　▽ 10

c)

Detail in d)

View in b)

500 m　N

Inferred inundation limit

d)

50 m　N

Detail in inset

Stranded ship

Destroyed pier

Remains of pier

7

8

Tsunami flow

Evacuation direction　Visual field of video **i**

e)

2018/09/28 18:06:33　219 s after the beginning of shaking (video 8)

People evacuating

Tsunami inundating

1
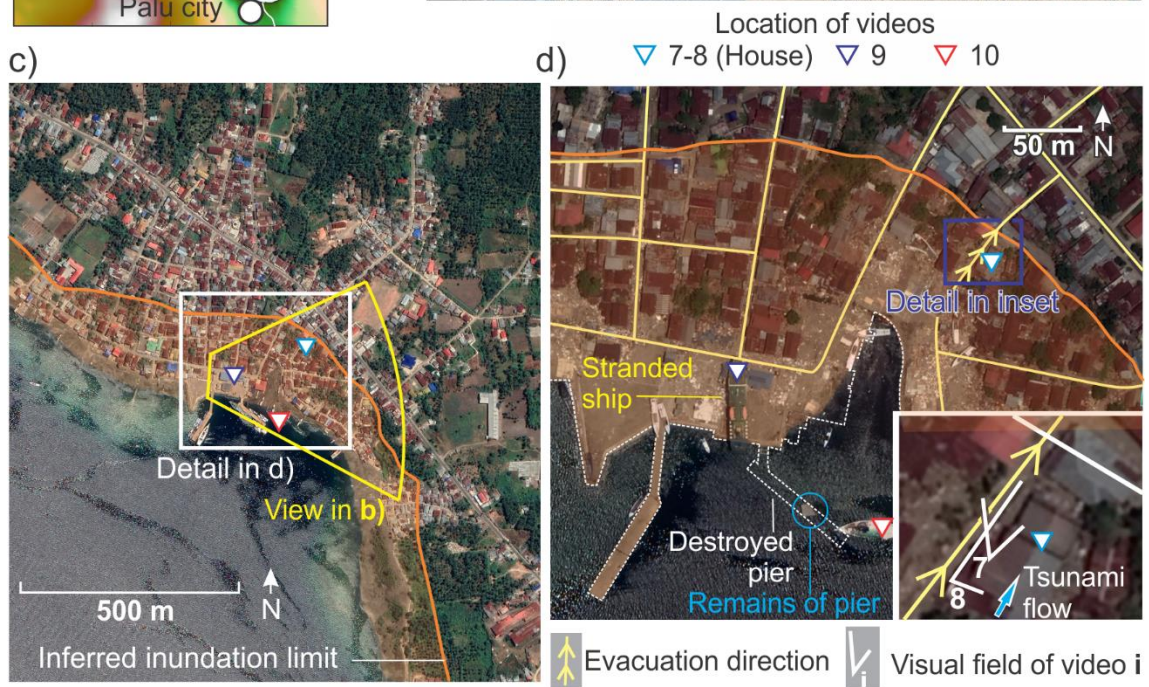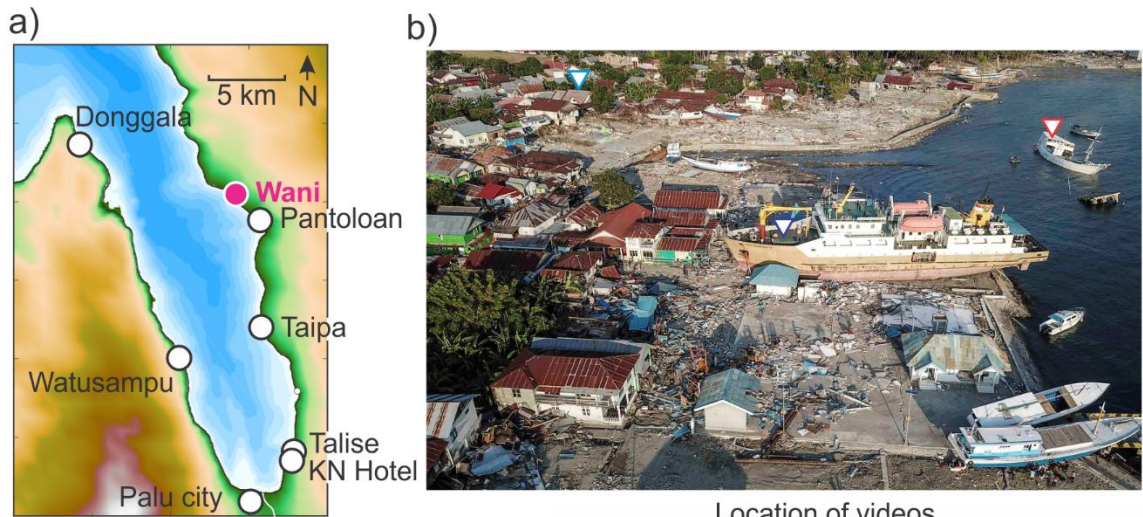
Figure S2. Video analyses at Wani. a) Map of Palu Bay and location of Wani. B) Aerial photo of Wani. Triangles indicate the location of the house (videos 7-8), stranded passenger ship (video 9) and moored fishing boat (video 10). c) Satellite image of Wani, showing the tsunami effect on the harbor (reported by crewmembers) and the inferred inundation area. d) Enlarged view of the study area, showing the local road configuration. The inset shows the house where CCTV videos 7-8 were taken, and the evacuation direction inferred from these. e) Snapshot of video 8 showing the direction of inundation relative to the evacuation road.

Figure S3. Video analyses at Pantoloan. a) Map of Palu Bay and location of Pantoloan. b) Satellite image of Pantoloan port, showing the inferred inundation area and the location and field of view of the CCTV camera (video 11) and video taken onboard the container ship (video 12). The location of the tide gauge station that recorded the tsunami (Fig. 1C) is shown by the red triangle. c) Snapshot from CCTV video 11 at a time

between the earthquake and tsunami. Note that the wharf has no signs of tsunami inundation and dust is likely coming from the collapse of a container crane. e-i) snapshots for video 11 from which the tsunami waveform was inferred. Tsunami amplitudes are inferred from actual dimensions of the KM Meratus Kendari 1, shown in j.
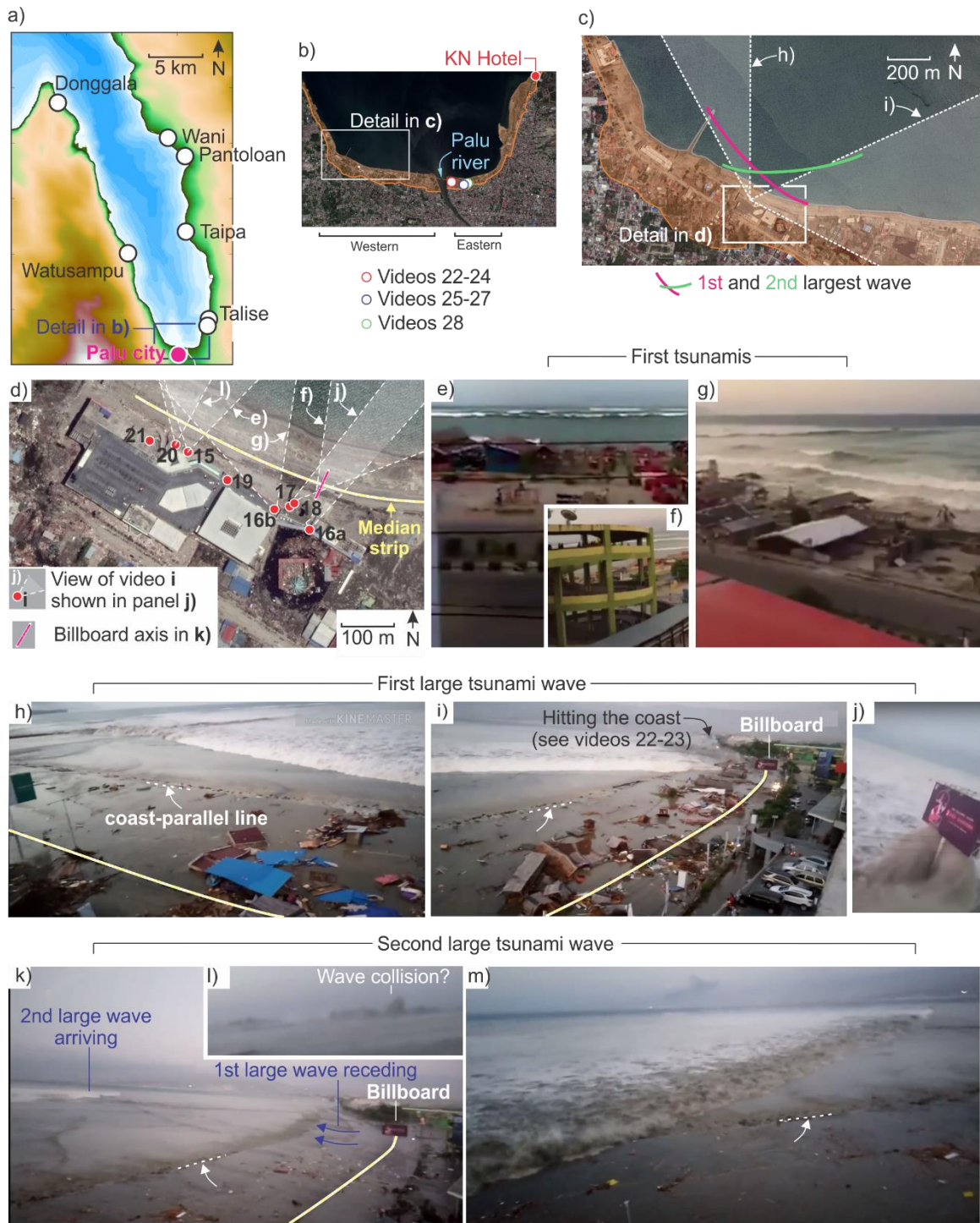
Figure S4. Video analyses at western Palu city. a) Map of Palu Bay and location of Palu city. b) Satellite image of the southern part of Palu Bay, indicating the inferred inundation area and the western and eastern sectors of Palu city. c) Close up of the western sector of the city showing the inferred inundation area, the video-inferred directions for the largest two waves and the fields of view of panels h) and i). d) Locations of the seven videos used for the analysis. g-i) Snapshots showing the first inundation phases, according to d).

(h-j) Snapshots showing the first large trailing wave (largest) observed at Palu city. A coast-parallel line is shown for reference. Note contrasting orientations of the wave fronts (h-i) and tsunami flow around the billboard post (j). (k,m) snapshots showing the second largest wave, according to d. (l) snapshot shows the collision of first and second trailing waves seen in video 20.
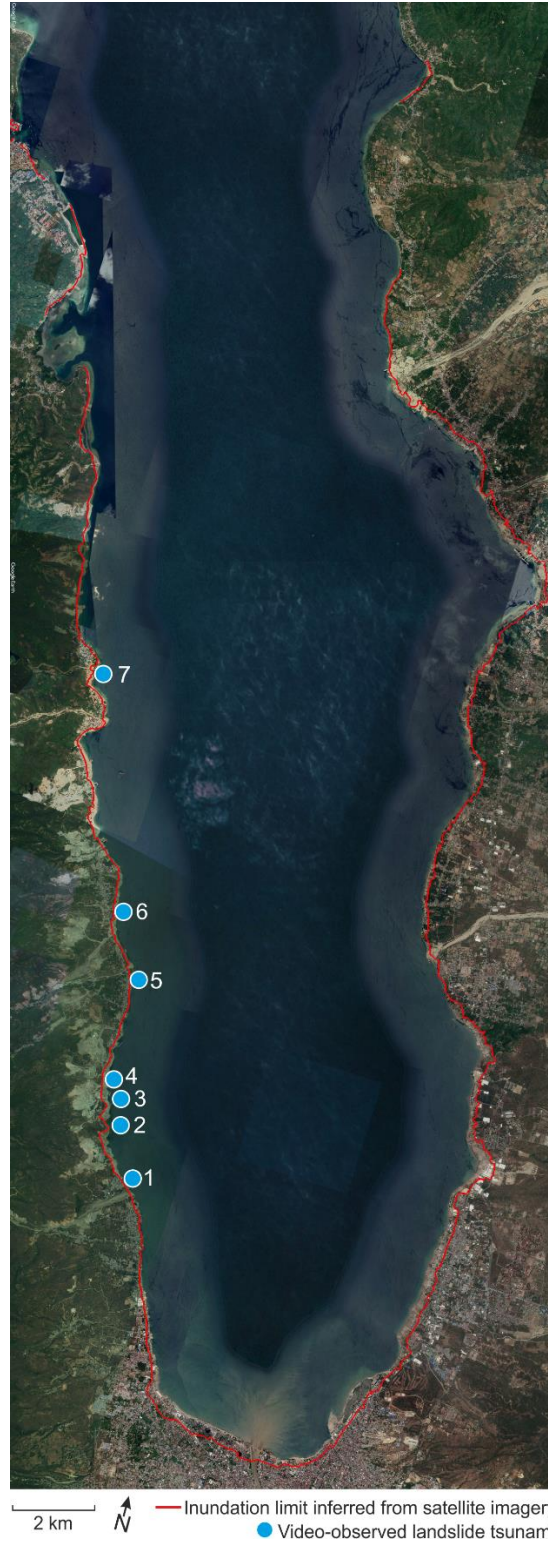
Figure S5. Inundation around Palu Bay inferred from detailed comparison of pre-and post-tsunami satellite images combined with amateur videos and photos. We inferred a maximum inland inundation of 420 m along the southeast coast of the bay.
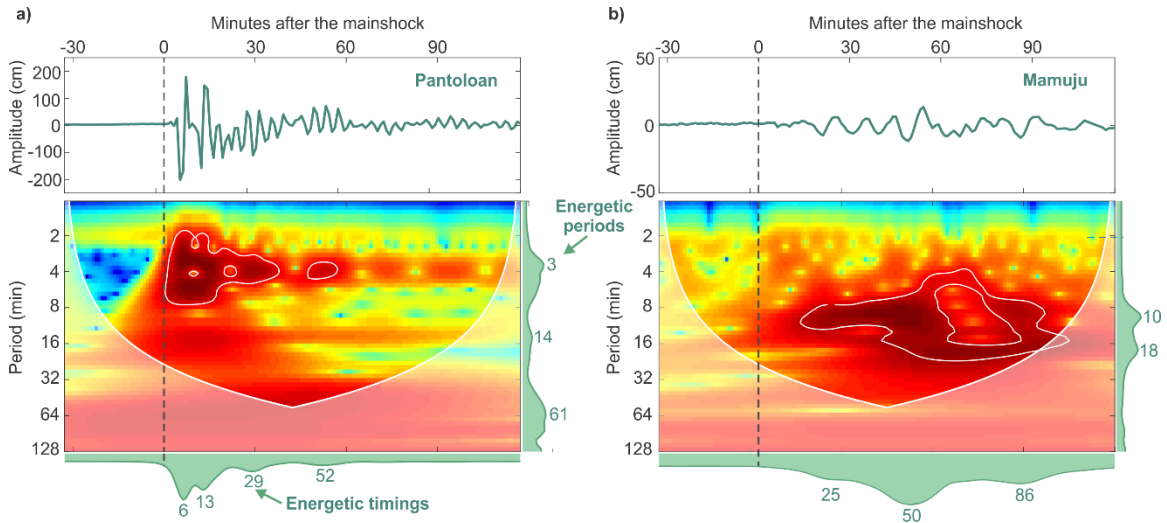
Figure S6. Time-frequency characteristics of the two tide gauge records available for the event: Pantoloan (a) and Mamuju (b) (Fig. 1C). Wavelet analysis was performed using the software package developed by Torrence and Compo (Torrence and Compo 1998), using a Morlet mother wavelet. Upper panels show the sea-surface elevation (η) of the de-tided signals. The lower panels show the Wavelet Power Spectra (WPS), in which white contours indicate the 95% confidence level. The green shaded regions at the right and below the WPS show the time-averaged and scale-averaged wavelet spectra, respectively, where numbers indicate energetic periods (in minutes) and arrival times (in minutes), respectively. Times are relative to the mainshock occurrence.
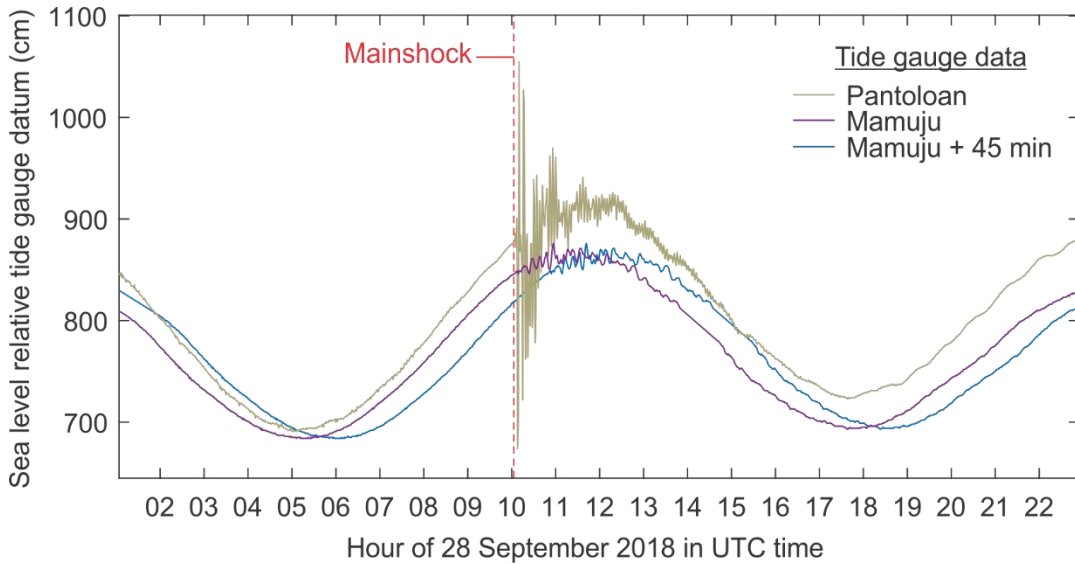
Figure S7. Comparison of the timing of the raw tide data recorded at Pantoloan (light brown) and Mamuju (purple). The blue curve is the Mamuju data delayed by 45 minutes as suggested by Heidarzadeh et al. (2018). Note that this time shift produces unrealistic differences in the tidal phases between Pantoloan and Mamuju which are 200 km apart. The time interval plotted corresponds to the day of the earthquake, 28 September 2018.
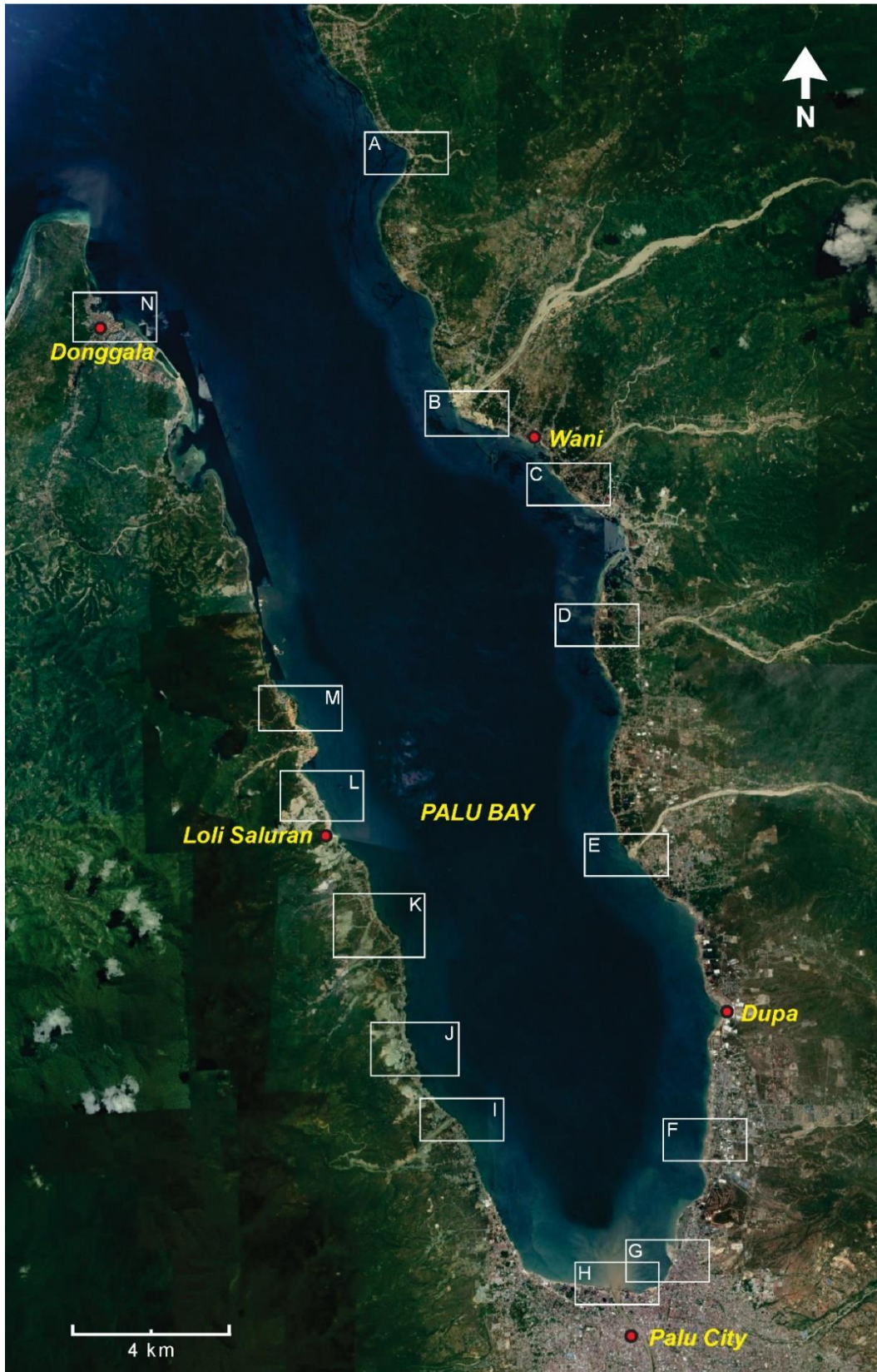
Figure S8

Figure S8 (cont.)

Figure S8 (cont.)

02/19/2018   10/01/2018

300 m   300 m

02/19/2018   10/01/2018

400 m   400 m

02/19/2018   10/01/2018

500 m   500 m

04/12/2016   10/01/2018

400 m   400 m
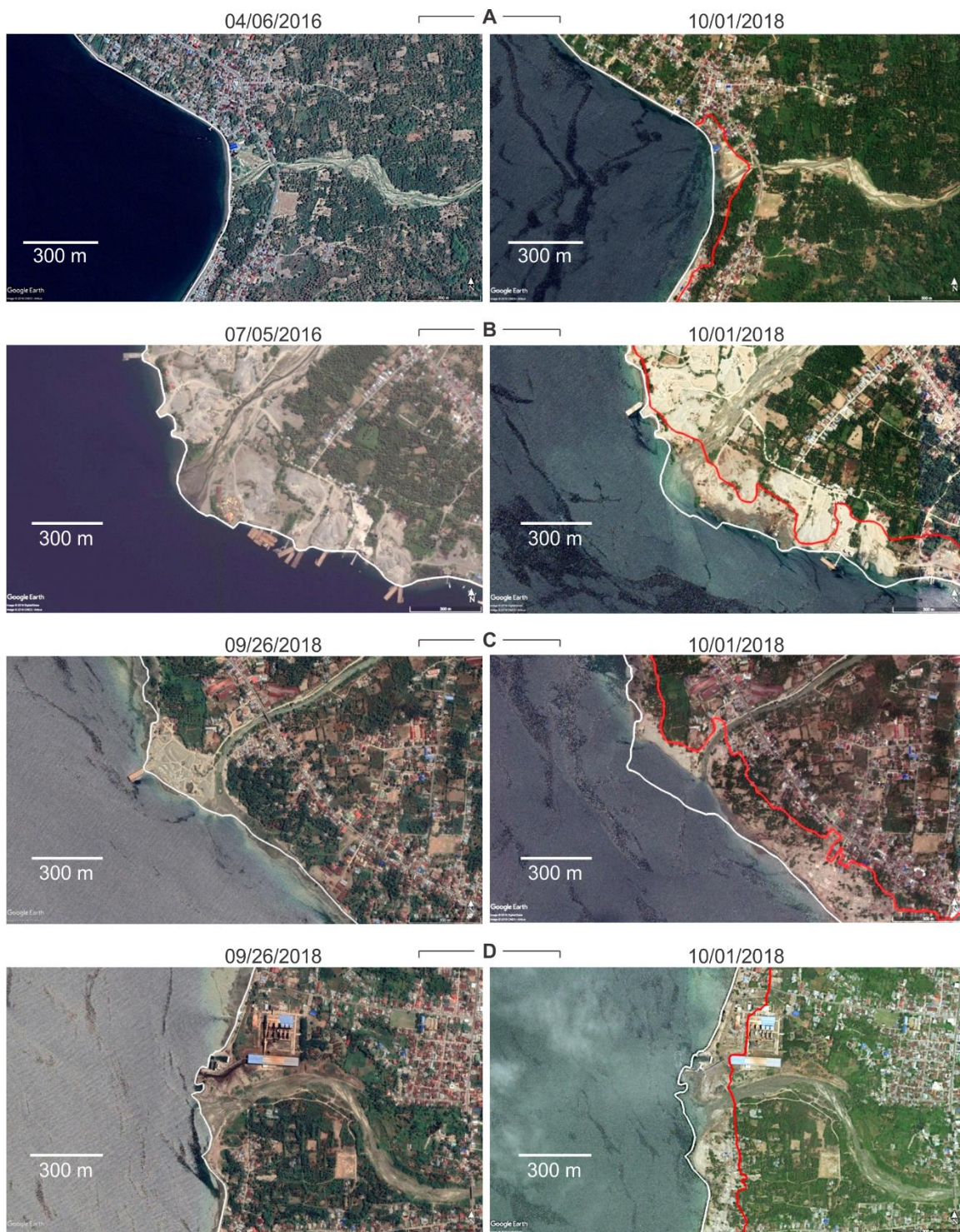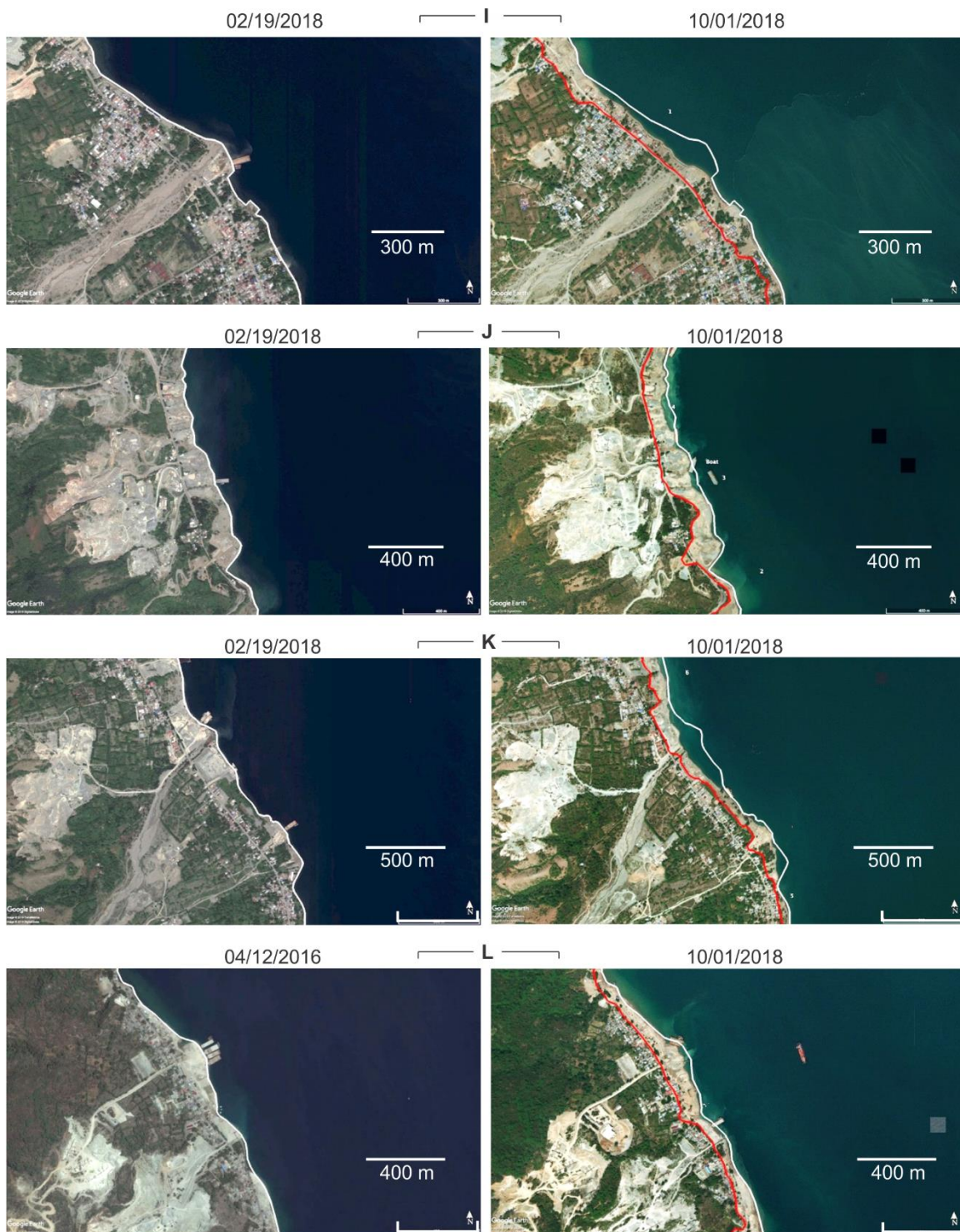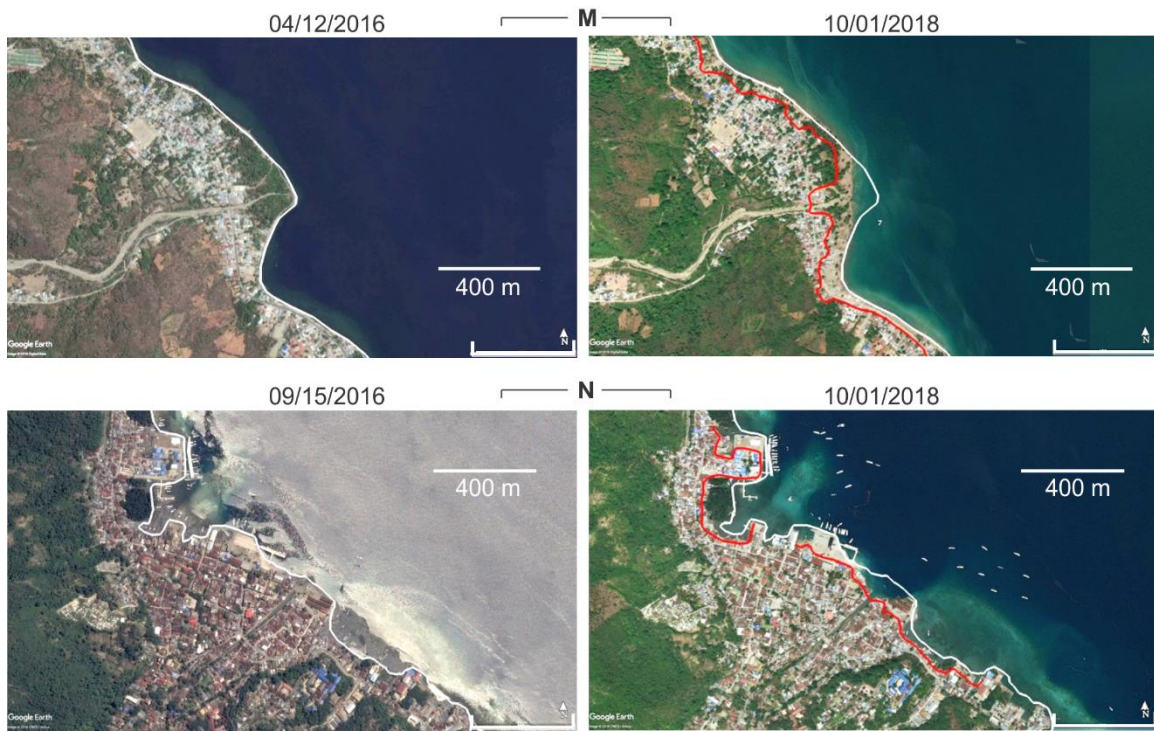
Figure S8 (cont.)

Figure S8 (cont.) Coastline retreat observations derived from the satellite image analysis. The first figure shows the index maps for areas in Palu Bay where coastal retreats were observed. The date of each pre-and post-earthquake photo is indicated above it. White lines indicate the pre-tsunami shoreline and the red line is the inferred inundation limit (see Fig. S5)

Table S1.

Video	Location	Type	Source
1	KN Hotel	CCTV	https://www.youtube.com/watch?v=M7Xl0JqjghM
2	KN Hotel	CCTV	https://www.youtube.com/watch?v=bhqdPhXcUv8
3	KN Hotel	CCTV	https://www.youtube.com/watch?v=IbFoRfImHKI
4	KN Hotel	CCTV	https://www.youtube.com/watch?v=seUK1AXTRSs&t=1s
5	KN Hotel	CCTV	https://www.youtube.com/watch?v=gSLWk3qUf74
6	KN Hotel	CCTV	https://www.youtube.com/watch?v=XsQaTvnas9s
7	Wani	CCTV	https://www.youtube.com/watch?v=8qaP7BCN87M&t=4s
8	Wani	CCTV	https://www.youtube.com/watch?v=SZSf-Uk4qmc&t=1s
9	Wani	Amateur	https://www.youtube.com/watch?v=WUdmR4D0r2w&t=223s
10	Wani	Amateur	https://www.youtube.com/watch?v=1sG0BPZBx-0&t=1s
11	Pantoloan	CCTV	https://www.youtube.com/watch?v=q2fCk4Qwvds
12	Pantoloan	Amateur	https://www.youtube.com/watch?v=DKoOGVGXP-A&t=6s
13	Talise	Amateur	https://www.youtube.com/watch?v=aAPfHEKPxBA
14	Dupa	Amateur	https://www.youtube.com/watch?v=vjbmtbHuHtI
15	West Palu city	Amateur	https://www.youtube.com/watch?v=mOEfs2Foh7E&t=21s
16	West Palu city	Amateur	https://www.youtube.com/watch?v=7GWNyxwVjJw
17	West Palu city	Amateur	https://www.youtube.com/watch?v=faz8Dz2HyJw&t=50s
18	West Palu city	Amateur	https://www.youtube.com/watch?v=zsF8WGtdlTk
19	West Palu city	Amateur	https://www.youtube.com/watch?v=hQhsXvfluho
20	West Palu city	Amateur	https://www.youtube.com/watch?v=ZAwSPTUYvKA
21	West Palu city	Amateur	https://www.youtube.com/watch?v=2djoExHDVac&t=129s
22	East Palu city	Amateur	https://www.youtube.com/watch?v=NUoup1EQKHE
23	East Palu city	Amateur	https://www.youtube.com/watch?v=iPjq_dPPUrM
24	East Palu city	Amateur	https://www.youtube.com/watch?v=pBfY8v4tpSY
25	East Palu city	Amateur	https://www.youtube.com/watch?v=xplXjWMf7QM&t=20s
26	East Palu city	Amateur	https://www.youtube.com/watch?v=vNhJb71i5UI
27	East Palu city	Amateur	https://www.youtube.com/watch?v=417rYUkNGcg
28	East Palu city	Amateur	https://www.youtube.com/watch?v=lIv0qXv5F_Q
29	Taipa	Amateur	https://www.youtube.com/watch?v=wB5mf6EZGYg
30	Taipa	Amateur	https://www.youtube.com/watch?v=KigPIhPxs6Y
31	Taipa	Amateur	https://www.youtube.com/watch?v=qoeAvUzA7JA
32	Watusampu	Amateur	https://www.youtube.com/watch?v=tjOB6mHBt4I
33	Donggala	Amateur	https://www.youtube.com/watch?v=_kIel6pV9nk

34	Loli Saluran Terminal	Amateur	https://www.youtube.com/watch?v=7RK98nLT7Hs&t=8s
35	BBM	amateur	https://www.youtube.com/watch?v=3z5DwOEdsdQ
36	Tipo	Amateur	https://www.youtube.com/watch?v=_uQF-YWVV1Q
37	Tipo	amateur	https://www.youtube.com/watch?v=OrbiZdcIWws
38	Pilot	Amateur	https://www.youtube.com/watch?v=c_qMXY4VsDQ
39	Boat	Amateur	https://www.youtube.com/watch?v=NNU1dUJOoKc&t=31s
40	High ground	Amateur	https://www.youtube.com/watch?v=cc4bEkNdse4
41	High ground	Amateur	https://www.youtube.com/watch?v=C9IjACZAxMo&t=1s
42	KN Hotel	compiled	Video 42 in online repository (Dataset S1)
43	Palu west	compiled	Video 43 in online repository (Dataset S1)

Location	Videos used to infer tsunami parameters			
	Direction	Arrival time	Period	Amplitude
KN Hotel	1-6	1-3	(-)	1-6
Wani	7-8	7-8	(-)	7-8
Pantoloan	(-)	11	11	11
Talise	(-)	13	(-)	(-)
Dupa	(-)	14*	(-)	14
West Palu city	15-21	15*	15-21	15-21
East Palu city	22-23	(-)	(-)	(-)

Table S2. Videos used to infer tsunami parameters at seven locations (Fig. 2A) and for waveform reconstructions at six location (Fig. 2B). For video codes refer to Table S1 and Dataset S1. * Arrival times include large uncertainties (see Text S1 for details). (-) Indicates that the parameter cannot be inferred from the videos. See compiled videos 42 and 43 for KN Hotel and West Palu city, respectively.

Dataset S1: Video collection used in this study. Video repository is at https://agsweb.ucsd.edu/tsunami/2018-09-28_palu/

Dataset S2: Video-inferred tsunami waveforms for six locations (Fig.2A)

.